

Structure and diffusion of active-passive binary mixtures in a single-file†

Tanwi Debnath^a, Shubhadip Nayak^b, Poulami Bag^b, Debajyoti Debnath^b and Pulak Kumar Ghosh^{b*}

^a *Department of Chemistry, University of Calcutta, Kolkata 700009, India and*

^b *Department of Chemistry, Presidency University, Kolkata 700073, India*

(Dated: March 15, 2023)

We numerically study structure and dynamics of single files composed of active particles, as well as, active-passive binary mixtures. Our simulation results show that when the persistent length of self-propelled particles is much larger than the average inter-particle separation and the self-propulsion velocity is larger than the thermal velocity, particles in the file exist as clusters of various sizes. Average cluster size and structures of the file are very sensitive to self-propulsion properties, thermal fluctuations and composition of the mixture. In addition to the variation of file composition, our study considers two sorts of mixture configurations. One corresponds to the uniform distribution of active passive throughout the mixture in the single file. In the other configuration, active particles are on one side of the file. For the both configurations, even a little fraction of active particles produces a large impact on the structure and dynamics of the file.

I. INTRODUCTION

Both in natural and biology inspired artificial nano-devices, diffusion under geometric constraints plays pivotal roles in controlling transports of key molecules/ions. In particular, the most often encountered situation is the diffusion of interacting particles through very narrow channels where particles cannot pass each other. Diffusion of interacting particles under such constraints occurs as a single-file. A tag particle in a single-file exhibits anomalous diffusion, where mean square displacement in the long time limits grows as, $\langle \Delta x^2 \rangle = \langle [x(t) - x(0)]^2 \rangle = 2D_\beta t^\beta$, with the exponent $\beta = 0.5$ for most general cases [1–5]. However, $\beta < 0.5$, as well as, $\beta > 0.5$ had also been reported for a tracer diffusion in a single-file [6, 7].

Historically, the idea of such non-Fickian diffusion of tag particles in a single-file was first introduced during studying transport of water molecules and ions through very narrow channels in membrane [8]. The theories of single file diffusion had been developed from different directions and revisiting the basic random walk problem under constraints in different contexts [2–5, 9–14].

Research on single file diffusion started gaining considerable attention with progress in synthesis of nano-materials, which made tracer diffusion in a single-file experimentally accessible. To be specific, synthetic zeolitic materials form networks of channels with radius little larger than the typical size of small organic molecules. Thus, transport of small molecules, like, methane and ethane through channel networks of zeolitic materials can be described as a single file diffusion. Experimental studies in such a system, using pulsed force gradient nuclear magnetic resonance, show that mean square displacement is directly proportional to $t^{1/2}$ [15, 16]. The most interesting trait of single-file diffusion, the transition from

the initial normal diffusion regime to the long-time limits sub-diffusion regime, has further been confirmed in the several experimental studies [17–19]. Moreover, single-file like sub-diffusive behavior is observed in diffusion of a tagged monomer in the active polymer [20, 21].

Some recent studies [22, 23] explore single-file diffusion of a new class of particles which can propel themselves by extracting kinetic energy from their surrounding medium. Such particles are known as active particles, can be of both natural origin (e.g., motor proteins, bacteria, microtubules, actin etc), as well as synthetic ones. Most common class of artificial active particles is the self-propelled Janus particles, consisting of two distinct hemispheres with different physical or chemical properties. Taking advantage of functional asymmetry, these active particles can induce either thermal or concentration gradients [24–29] to propel themselves. Due to self-propulsion mechanisms, active particles are typical non-equilibrium systems [30, 31] with huge application potential for nano-technology and biomedical sciences.

In this paper, we explore structural and dynamical properties of a system of interacting active particles, as well as, active-passive binary mixture with varying composition in a single-file. To examine impact of motile active particles in the diffusion of sluggish passive ones, we consider two different file configurations: (1) all the active particles are uniformly distributed over the chain [see Fig. 1(b)]; (2) Active particles are in the one end of the 1D-chain, and the other end contains passive particles only [see Fig. 1(c)]. Our numerical results show that for both types of configurations, even for small concentrations of the active particles the mixture behaves like a system of interacting active particles. Further, particles in the mixture preferably exist as clusters of various sizes for large persistence length of self-propulsion. Diffusion of tagged particles in the single file enhances monotonically with increasing fraction of active particles in the mixture. All these features attribute to motility transfer from the energetic active particles to the slowly moving passive ones.

We organize the contents of this paper as follows.

*Email: pulak.chem@presiuniv.ac.in

† This paper is dedicated to 75th Birth Anniversary of Professor S. P. Bhattacharyya

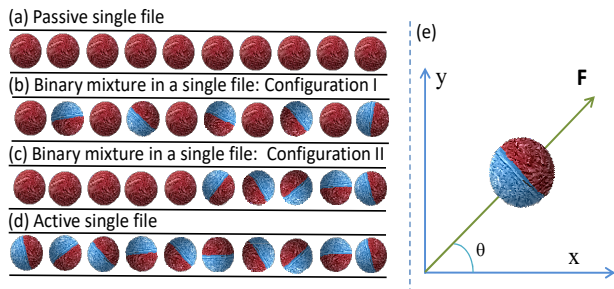


FIG. 1: (Color online) Schematics for single-file in a 1D narrow channel: (a) Single file of passive particles; (b) *Configuration -I*: Single file containing active-passive binary mixture where active particles are uniformly distributed over the entire mixture; (c) *Configuration -II*: File contains binary mixture where active particles occupy one half and other half of the file is filled with passive particles; (d) File comprises active Janus particles; (e) Schematic of a Janus particle depicting direction of the self-propulsion force \mathbf{F} (modulus F_0) with respect to the channel axis.

Section 2 introduces the key ingredients of the model for a single file: the inter-particle interaction potential ensuring non-passing constraints, and the particle self-propulsion mechanism and associated parameters. In Sec. 3.1, we explore the structure of an active single file both in the thermal and athermal conditions. File structure of active-passive binary mixtures with varying configuration and composition has been investigated in the Sec. 3.2. Section 4 analyses diffusion of single-files. Finally, in Sec. 5, we summarize our results and draw a few relevant concluding remarks considering the future direction of work.

II. MODEL

We consider a binary mixture of N_a active and N_p passive particles in a single file. Fractions of the active and passive particles in the mixture are, $\eta_a = N_a/(N_a + N_p)$ and $\eta_p = N_p/(N_a + N_p)$, respectively. Active particles are characterized by their self-propulsion velocity, v_0 and its persistence time, τ_θ . Further, all particles, $N = N_a + N_p$, are represented by disks of radius r_0 and they interact with each other via a truncated Lennard-Jones (L-J) potential. The interaction energy (V_{ij}) between a pair of particles separated by a distance r_{ij} is given by,

$$V_{ij} = 4\varepsilon \left[\left(\frac{\sigma}{r_{ij}} \right)^{12} - \left(\frac{\sigma}{r_{ij}} \right)^6 \right], \text{ if } r_{ij} \leq r_m$$

$$= 0 \text{ otherwise,} \quad (1)$$

where r_m locates the potential minimum and σ is the diameter of the particle. Dynamics of a tagged particle in the single file can be described by the following set of

overdamped Langevin equation,

$$\gamma \dot{x}_i = \sum_j F_{ij} + F_{0,i} \cos \theta_i + \xi_i^x(t),$$

$$\dot{\theta}_i = \xi_i^\theta(t). \quad (2)$$

Where, γ is the damping strength depending on the particle's size and viscosity of the medium. The i -th particle at the position x_i encounters inter-particle repulsive interaction $\sum_j F_{ij}$ [derived from Lennard-Jones potential (1)] with its neighbouring ones. This force does not allow particles to pass each other. In addition to these interactions, particle motion is governed by the combined action of self-propulsion and equilibrium thermal fluctuations.

For active particles we consider self-propulsion velocity ($\mathbf{v}_{0,i} \equiv \mathbf{F}_i/\gamma$) with a constant modulus v_0 ($\equiv F_{0,i}/\gamma$). On the other hand, $\mathbf{v}_{0,i} = 0$ for passive particles. The self-propulsion velocity $\mathbf{v}_{0,i}$ is oriented at an angle θ_i with respect to the x -axis [as depicted in Fig. 1(e)]. However, the direction (θ) changes due to rotational diffusion described by the Wiener process of Eq.(2), where $\langle \xi_i^\theta(t) \rangle = 0$ and $\langle \xi_i^\theta(t) \xi_j^\theta(t') \rangle = 2D_\theta \delta_{ij} \delta(t - t')$. The rotational diffusion constant D_θ is related to the persistence time and length of self-propulsion velocity as, $\tau_\theta = 1/D_\theta$ and $l_\theta = \tau_\theta v_0$, respectively. From the correlation function, $\langle \cos \theta_i(t) \cos \theta_i(0) \rangle = \langle \sin \theta_i(t) \sin \theta_i(0) \rangle = (1/2) \exp[-D_\theta |t|]$, it is apparent that D_θ coincides with the rotational relaxation rate of the self-propulsion velocity $\mathbf{v}_0(t)$.

The last term in the Eq. (2) represents zero mean, delta-correlated, $\langle \xi_i^x(t) \xi_j^x(0) \rangle = 2D_0 \gamma^2 \delta_{ij} \delta(t - t')$ thermal fluctuations with Gaussian distribution. Where, D_0 is the free space diffusion constant in the absence of self-propulsion.

For a passive particle, both the rotational diffusion and translational diffusions are of thermal origin. For a spherical colloidal particle of radius r_0 , the rotational and translational diffusion constants in a medium with viscosity η_v and at the temperature T , can be expressed as, $D_\theta = k_B T / 8\pi \eta_v r_0^3$ and $D_0 = k_B T / 6\pi \eta_v r_0$, respectively. However, for an active particle rotational diffusion can also depend on the mechanisms fueling its self-propulsion. For this reason, v_0 , D_θ and thermal diffusion constant D_0 are treated here as independent model parameters [26, 32, 33].

The coupled equations (2) have been numerically integrated using a standard Milstein algorithm [34] to explore structure of the active-passive mixture as well as diffusion of a tagged particle in the single files. Specifically, we estimate the fraction of particles form cluster, cluster size, and the mean square displacement of a tagged particle. The numerical integration has been performed using a very short time step, $10^{-5} - 10^{-6}$, to ensure numerical stability. At $t = 0$, we assume all particles are uniformly distributed in the 1D box of length L with random orientation of self-propelled velocity \mathbf{v}_0 . To keep the mixture density constant with respect to both active and passive species we use periodic boundary conditions.

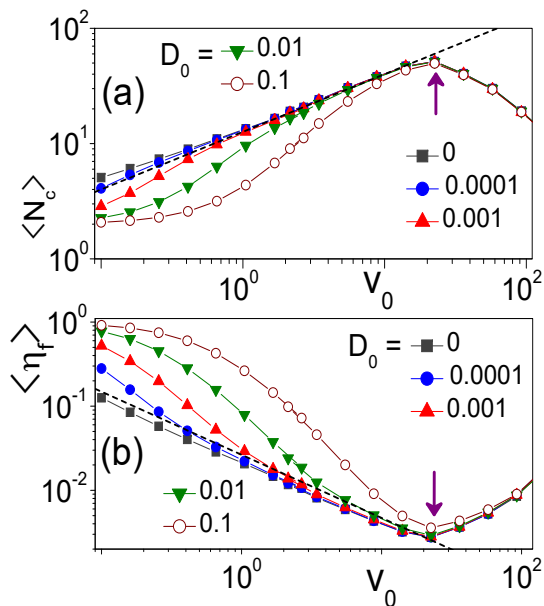


FIG. 2: (Color online) (a) Average particle number in a cluster $\langle N_c \rangle$ as a function of self-propulsion velocity v_0 for different thermal diffusion constant D_0 (see legends). (b) Average fraction of particles exist as a single particle ($\langle \eta_f \rangle$) in the mixture versus v_0 for different D_0 as shown in the legends. The dashed lines in (a) and (b) correspond to the Eq.(3) and Eq.(5), respectively. The remaining model parameters are (unless reported otherwise in the legends): $D_\theta = 0.002$, and $\rho_N = 0.16$.

In our simulation we choose particle diameter σ as the unit of length. The unit time and force, respectively, are defined as, $\gamma\sigma^2/\varepsilon$ and ε/σ . Throughout this paper, we set $\varepsilon = 1$, $\gamma = 1$, and $\sigma = 1$.

III. SINGLE FILE STRUCTURE

We first explore the structure of active-passive binary mixture in a single file. Our simulation results reveal that particles in the mixture exist as clusters of various sizes as long as self-propulsion length (l_θ) surpasses the average separation between two adjacent particles. Similar to the earlier results [35–42] for higher dimensions, in one dimension the formation of aggregates is solely attributed to the motility of active particles and interparticle attractive forces play no role. Such an interesting phenomenon is referred to as motility induced phase separation.

To characterize structure of the mixture we numerically estimate average cluster size, average fraction of particles exist as single and cluster size distributions. We assume two particles form a cluster whenever their centre to centre distance is less than the cut-off distance r_m where particles start encountering repulsive force. Clusters are counted in the long time limits where effects of transient processes can safely be ignored. Average cluster size, *i.e.*, average number of particles in a cluster ($\langle N_c \rangle$)

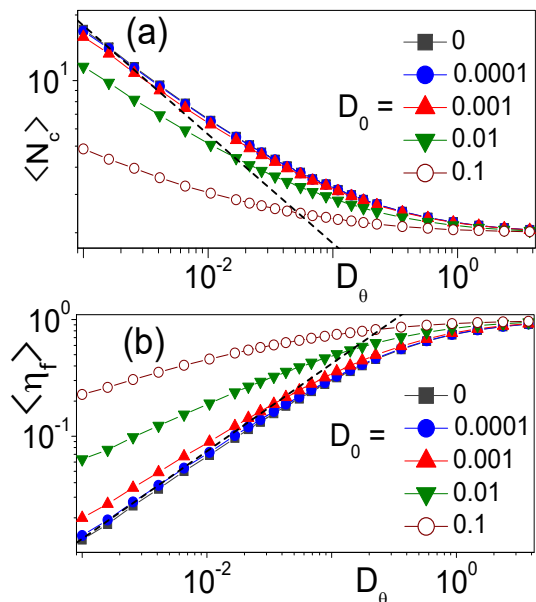


FIG. 3: (Color online) (a) $\langle N_c \rangle$ vs. D_θ and (b) $\langle \eta_f \rangle$ vs. D_θ for different thermal diffusion constant D_0 (see legends). The dashed lines in (a) and (b) correspond to the Eq.(3) and Eq.(5), respectively. The remaining model parameters are (unless reported otherwise in the legends): $v_0 = 1.0$, and $\rho_N = 0.16$.

is estimated by taking average over as many as 1000 observations. The time lag between two observations is chosen to be much larger than the rotational relaxation time τ_θ .

A. Structure of an active single file

In Fig. 2(a,b) and Fig. 3(a,b) we present the average cluster size and the average fraction of particles which does not form cluster ($\langle \eta_f \rangle$) as a function of self-propulsion parameters in the limit, $\eta_a \rightarrow 1$. It is apparent from simulation results that thermal noise has a strong impact on the structure of the file. When the self-propulsion contribution in the diffusion is much stronger than thermal diffusion, $v_0^2/2D_\theta \gg D_0$, the average cluster size $\langle N_c \rangle$ grows linearly with the square root of self-propulsion velocity, rotational relaxation time and particle number density. Average cluster size can be expressed in more general empirical relation,

$$\langle N_c \rangle = A (v_0 \rho_N \tau_\theta)^{\beta_1} \quad (3)$$

where, $\beta_1 \sim 1/2$ in the athermal condition. Further, ρ_N is the particle density and its reciprocal is the average interparticle separation. This is in accord with the earlier report [23]. The pre-factor A is a constant and it is close to $\sqrt{2}$ for the best fitting numerical data. Note that Eq. (3) is valid as long as self-propulsion persistence length is much larger than the average inter particle spac-

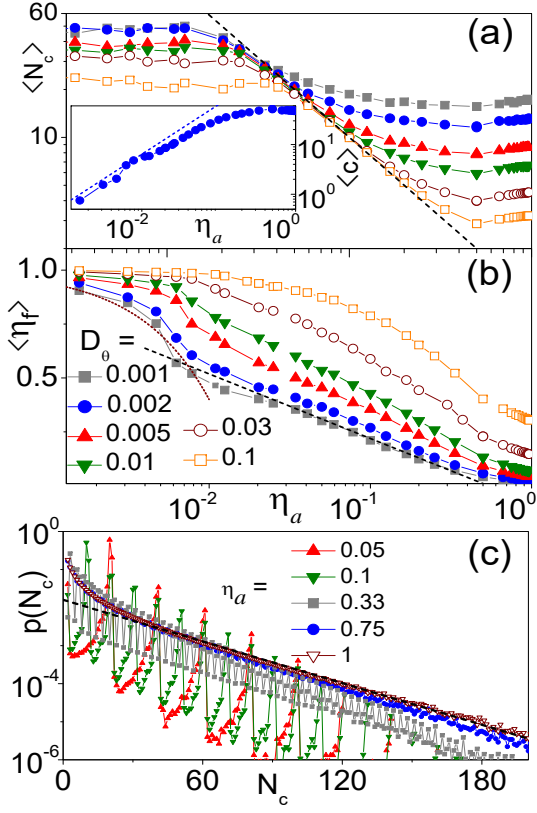


FIG. 4: (Color online) (a) $\langle N_c \rangle$ vs. η_a for different rotational diffusion constant D_θ (see legends) when active particles are uniformly distributed over the entire length of the file (*configuration-I*). The dashed line displays Eq.(7). Inset depicts average cluster numbers $\langle c \rangle$ as a function of η_a . Dashed line here indicates that the average cluster number is equal to the number of active particles ($\langle c \rangle = N\eta_a$). (b) Similar figure as (a) but $\langle \eta_f \rangle$ vs. η_a . The dotted line represents Eq.(9). The dashed line is a guide to the eye showing logarithmic decay of the form: $\langle \eta_f \rangle = A_1 + B_1 \ln(\eta_a)$, where A_1 and B_1 are functions of self-propulsion parameters. (c) Cluster size distribution with varying mixture composition (see legends). The dashed line is the estimation of exponentially decaying tail based on the Eq.(10). The model parameters are (unless reported otherwise in the legends): $v_0 = 1.0$, $\rho_N = 0.16$, $D_0 = 0$, and $D_\theta = 0.002$.

ing, $l_\theta \gg 1/\rho_N$ and self-propulsion strength is not too strong.

Figure 2(a) shows that beyond a certain threshold value of the self-propulsion velocity, the cluster size monotonically decays with v_0 . This is due to the fact that with growing self-propulsion force, penetration length of the self-propellers increases leading to decrease of the effective particle size. Thus, the density of the system gradually decays with v_0 . The penetration length can be estimated by equating repulsion force due to L-J potential with the self-propulsion force, $dV/dr + F_0 = 0$. When two particles touch each other, $|x_i - x_j| = \sigma$, the force

balance condition produces the threshold value of v_0 ,

$$v_0^c = \frac{24\epsilon}{\sigma} \quad (4)$$

When, $v_0 > v_0^c$, particles' self-propulsion force becomes strong enough to penetrate each other overcoming repulsive interaction derived from L-J potential. This leads to a drop of the effective density of the system. Thus, one can expect a change in the trend of variation for $\langle N_c \rangle$ vs. v_0 and $\langle \eta_f \rangle$ vs. v_0 around $v_0 = v_0^c$.

Simulation results in Fig.2 well corroborate above reasoning. $\langle N_c \rangle$ versus v_0 displays a maximum and $\langle \eta_f \rangle$ versus v_0 exhibits a minimum around $v_0 = v_0^c$. This estimation is indicated by vertical arrows [see Fig. 2(a, b)].

Both in the thermal and athermal conditions, $\langle \eta_f \rangle$ monotonically decays with self-propulsion parameters, v_0 and τ_θ , as well as ρ_N when $v_0 < v_0^c$. Our simulation results show that for $D_0 = 0$ and $l_\theta \gg 1/\rho_N$ following empirical relation holds,

$$\langle \eta_f \rangle = B \left(\frac{1}{v_0 \tau_\theta \rho_N} \right)^{\beta_2} \quad (5)$$

Simulation data in Fig.2(b) and Fig.3(b) are best fitted for $B = 1/2^{\beta_2}$ and $\beta_2 = 0.75$. Estimation based on the empirical relation [Eq. (5)] is indicated by a dashed line. As anticipated, when the self-propulsion length is comparable or much smaller than the inter-particle spacing, $l_\theta \sim 1/\rho_N$, the equation (5) loses its validity. In this limit, the self-propellers change their direction before they travel an appropriate distance to collide and form clusters. Thus, $\langle N_c \rangle$ and $\langle \eta_f \rangle$ become insensitive to the particle's rotational dynamics as long as, $D_\theta \gg \rho_N v_0$. Further, in this regime, cluster formation becomes a rare event due to frequent flipping of self-propulsion velocity direction. If an aggregate happens to form, there would be overwhelmingly more probability for the two-particle clusters than that of other sizes. Thus, for the vanishingly small rotational relaxation time, $\langle N_c \rangle \rightarrow 2$ and $\langle \eta_f \rangle \rightarrow 1$.

We conclude this section with notes on the impact of the thermal translational diffusion on, $\langle N_c \rangle$ and $\langle \eta_f \rangle$. Simulation results in Fig. 2 and Fig. 3 show that thermal fluctuations even of very little intensity ($D_0 \ll v_0^2/2D_\theta$, as well as, $v_0 \gg \sqrt{\gamma D_0}$) have noticeable impact on the file structure. As usual, the thermal noise destroys the order structure, $\langle N_c \rangle$ monotonically decays, whereas, $\langle \eta_f \rangle$ enhances with thermal noise strength. When the average thermal velocity ($v_{th} = \sqrt{\gamma D_0}$) is comparable or larger than v_0 , the structure of the file remains insensitive to the self-propulsion parameters.

B. Structure of binary mixture in a single file

In a passive single file, particles are almost uniformly distributed with an average interparticle separation $l_s =$

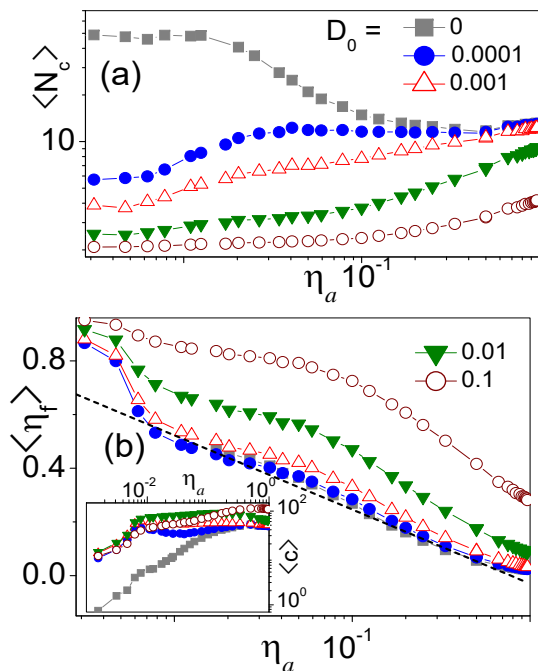


FIG. 5: (Color online) (a) $\langle N_c \rangle$ vs. η_a , and (b) $\langle \eta_f \rangle$ vs. η_a for different thermal diffusion constant D_0 (see legends) when active species are uniformly distributed over the entire length of the file (*configuration-I*). The dashed line in panel (b) guides to the eye showing logarithmic decay similar as in Fig. 4(b). Further, the inset in the panel (b) shows average cluster number versus η_a . The model parameters are (unless reported otherwise in the legends): $v_0 = 1.0$, $\rho_N = 0.16$, and $D_\theta = 0.002$.

$1/\rho_N$. Now, with gradually introducing active particles the structure of the file changes drastically. Active particles push the sluggish passive ones and form aggregates of different sizes. For a systematic analysis, we consider two possible configurations of the binary mixtures. *Configuration I*: Active particles are uniformly distributed throughout the mixture [see Fig.1(b)]; *Configuration II*: Active particles are in the one side of the file and the other side contains passive particles only (see Fig.1(c)).

For the both configurations, for a vanishingly small fraction of active particles in the mixture very large clusters are formed however they are very few in number. Noticeably, the structure of $\langle N_c \rangle$ versus η_a , average cluster number ($\langle c \rangle$) over the length L versus η_a , and $\langle \eta_f \rangle$ versus η_a are considerably different for two configurations, as well as, they are very sensitive to the thermal fluctuations [see Fig. (4-7)].

Configuration I: Active particles are uniformly distributed throughout the mixture

Athermal regime — Here we begin our discussion considering the situation of zero thermal fluctuations ($D = 0$). Figure 4 shows that in the athermal condition, the average cluster number is equal to the number of the active

particles in the mixture. It produces, $\langle c \rangle \sim N_a = \eta_a N$ (indicated by the dashed line in the inset of Fig.4(a)). Where, N_a is the number of active particles in the mixture. However, the cluster size $\langle N_c \rangle$ remains insensitive to η_a as long as the dynamics of an active particle is not affected by other active particles. Injected active particles push all the passive ones they encounter in their path and form a cluster. Suppose, an active particle is injected in a system of passive particles with average separation l_s . Further, we assume that the active particle is oriented along the channel axis at the starting point and it moves with an average velocity $\bar{v} = 2v_0/\pi$ until its direction reverts by diffusing over an angle π . These assumption yields particles in the aggregate,

$$\langle N_c \rangle = \sqrt{\frac{2\pi v_0}{l_s D_\theta} + \frac{1}{4}} - \frac{1}{2} \quad (6)$$

As time elapses the system loses its structural uniformity and cluster size changes drastically. This is due to the fact that even when the active pusher reverts its direction the passive particles remain close to each other due to the absence of the thermal fluctuations. Thus, in the next turn when the active particle encounters this closely spaced passive crowd, the cluster would form aggregating more particles. Further, on reverting direction the active particle gets a long free run to reach the passive crowds fast. Therefore, the average cluster size, $\langle N_c \rangle$, in the long time limit is considerably different from the Eq. (6).

With gradually adding active particles in the mixture, after a certain critical concentration, when separation between two adjacent active particles is close enough to interfere with each other's dynamics, the average cluster size decreases with η_a . As expected, this critical concentration is sensitive to the self-propulsion length. The transition point in Fig. 4(a) moves to the large η_a in going from the low to high rotational diffusion. In this regime total passive particle sequences are equally divided by active pushers. Each segment behaves as a cluster with average size,

$$\langle N_c \rangle \sim N/N_a = 1/\eta_a. \quad (7)$$

This estimation [indicated by dashed line in Fig. 4(a)] well corroborates simulation results.

When active species concentration is high enough, the mixture behaves like an active single file. In this region, both the cluster number and cluster size become independent of the η_a . For $\eta_a \rightarrow 1$, one recovers Eq. (3).

Figure 4(b) displays variation of the average fraction of the particles that survive as a single. It can be estimated as,

$$\langle \eta_f \rangle = \frac{N - \langle c \rangle \langle N_c \rangle}{N} \quad (8)$$

Recall that in the limit $\eta_a \rightarrow 0$, the $\langle c \rangle$ is equal to the number of the active particle in the system. Further, $\langle N_c \rangle$ is independent of the mixture composition. This yields,

$$\langle \eta_f \rangle = 1 - \eta_a \langle N_c \rangle \quad (9)$$

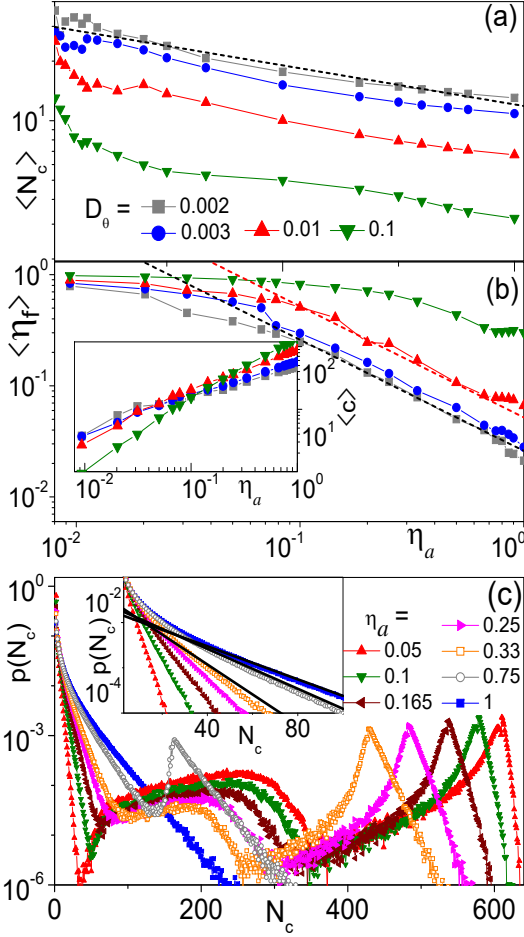


FIG. 6: (Color online) (a) $\langle N_c \rangle$ vs. η_a for different rotational diffusion constants D_θ (see legends) when active particles are added from one side of the file (*configuration-II*). The dashed line displays an eye guide for exponential decay. (b) Similar figure as (a) but $\langle \eta_f \rangle$ vs. η_a . The dashed line represents the inverse relation between average fraction of free particles and active fraction in the mixture ($\langle \eta_f \rangle \sim 1/\eta_a$). Inset depicts average cluster numbers $\langle c \rangle$ as a function of η_a . (c) Cluster size distribution with varying mixture composition (see legends). Inset is the distribution for small cluster size regime showing exponential decay tails. The solid black line is the estimation of exponentially decaying tail based on the Eq. (10), with the substitution of ρ_N by $\bar{\rho}_N$ (see text). Other model parameters are (unless reported otherwise in the legends): $v_0 = 1.0$, $\rho_N = 0.16$, $D_0 = 0$, and $D_\theta = 0.002$.

Estimation based on the above equation [dotted line in the Fig.4(b)] accords with the simulation data. For quite a high active particle concentration $\langle \eta_f \rangle$ is very low and it exhibits a logarithmic decay with η_a .

Cluster size distribution — To better understand the structure of the binary mixture we examine cluster size distribution, $p(N_c)$, with varying file composition. For $\eta_a \rightarrow 1$, $p(N_c)$ monotonically decays with N_c . In the athermal condition, numerical results in Fig.4(c) witness fast (for small N_c) and slow (for large N_c) decaying seg-

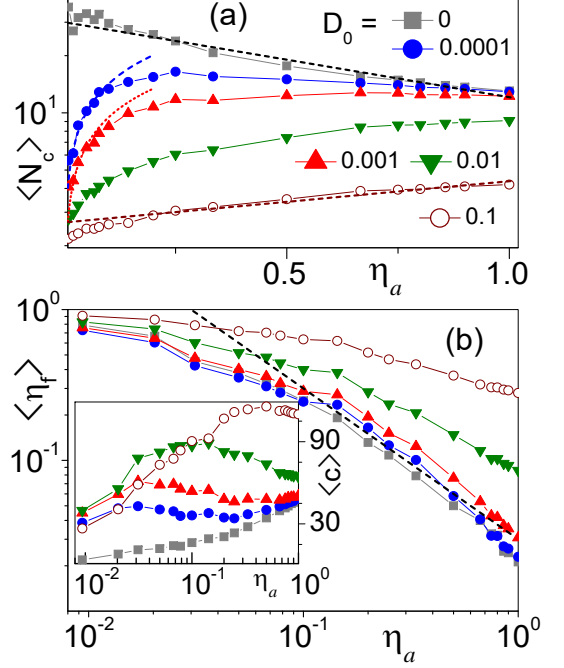


FIG. 7: (Color online) (a) $\langle N_c \rangle$ vs. η_a for different thermal diffusion constants D_0 (see legends) when active particles are added from one side of the file (*configuration-II*). The dashed line displays an eye guide for exponential decay. (b) Similar figure as (a) but $\langle \eta_f \rangle$ vs. η_a . The dashed line represents the inverse relation between average fraction of free particles and active fraction in the mixture ($\langle \eta_f \rangle \sim 1/\eta_a$). Inset depicts average cluster parameters $\langle c \rangle$ as a function of η_a . The remaining simulation parameters are (unless reported otherwise in the legends): $v_0 = 1.0$, $\rho_N = 0.16$, and $D_\theta = 0.002$.

ments in $p(N_c)$. The long tail decaying part is apparently exponential. However, the distribution function considerably deviates from, $(1/\langle N_c \rangle) \exp[-N_c/\langle N_c \rangle]$, due to contribution of the initial fast decaying segment. The decaying tail of the distribution can be represented as,

$$p(N_c) \sim \exp \left[-\frac{CN_c}{\sqrt{v_0 \rho_N \tau \theta}} \right] \quad (10)$$

The above equation is best fitted with simulation results [in Fig.4(c)] for $C = 0.38$. With the introduction of passive particles noticeable changes in the size distribution are: (i) the tail of $p(N_c)$ decays faster, and (ii) an oscillating component around the decaying tail emerges.

With decreasing η_a the effective self-propulsion velocities of the active species get suppressed as they move pushing passive particles. It follows from Eq.(10) that decaying tails become steeper with decreasing v_0 .

The periodic structure of the distribution becomes clearly noticeable when $\eta_a \leq 1/2$. For this mixture composition, each active swimmer encounters $(1 - \eta_a)/\eta_a$ passive particles on their either side. As a result, an active particle aggregating passive ones forms a cluster of size, $N_c = (1 - \eta_a)/\eta_a + 1 = 1/\eta_a$. Further, two or more such clusters can be aggregated to form larger

clusters. This produces peaks of $p(N_c)$ at $N_c = m/\eta_a$, with $m = 1, 2, 3, \dots$. When η_a is neither too small (such that huge passive particles in between two swimmers can not be aggregated by pushing action) nor too large, the height of the first peak is much larger than the other peaks. In this regime, the most probable peak position $N_c = 1/\eta_a$ coincides with the average cluster size. This estimation accords with Eq. (7).

Effects of the thermal fluctuations — The presence of the thermal fluctuations leads to a considerable structural change of the file. It is manifested in the variation of $\langle c \rangle$, $\langle N_c \rangle$ and $\langle \eta_f \rangle$ with changing the mixture composition. It is apparent from the Fig. 5, the thermal fluctuations break the large clusters into a number of smaller segments. Thus, for the very little fraction of the active particles in the mixture, the clusters are much smaller, however, they are more in number in comparison to the corresponding athermal limits. Nevertheless, similar to the athermal condition, the cluster size remains insensitive, and the cluster number linearly grows with the increase of active particle's concentration.

Beyond the critical concentration, when an active particle starts encountering impact of self-propulsion of the adjacent particles, depending upon the strength of the thermal fluctuations, the $\langle c \rangle$ decays very slowly or remains unchanged with η_a . Further, the cluster size very slowly increases with increasing η_a . This is in sharp contrast to the athermal limit where $\langle c \rangle$ and $\langle N_c \rangle$ keep growing and decaying, respectively, with increasing η_a unless active particle concentration is too high. For the very high concentration of the active particles, the mixture behaves alike both in the thermal and athermal limits.

Figure 5(b) depicts that $\langle \eta_f \rangle$ exhibits similar variation with η_a as in the athermal situations unless the strength of the thermal fluctuations is too large. This attributes to the fact that the key quantity, $\langle c \rangle \langle N_c \rangle$, which determines the value of $\langle \eta_f \rangle$, remains unchanged despite the splitting of the large clusters into smaller pieces due to thermal fluctuations.

Configuration II: Active particles are in the one side of the file

We now consider the situation where active particles are added from one end of the file. Such situations may be encountered in cleaning micro-channels using self-propelled particles. In contrast to the *configuration I*, here two types of clusters, pure active and active-passive, can also be formed. Further, passive particles are pushed either by a single active or cluster of n active particles with their centre of mass velocity $v_c = \sum_{i=1}^n v_i/n$. The velocity of the active cluster can be varied from its minimum, $v_c = 0$, to the maximum $v_c = v_0$. The cluster centre of mass velocity is a function of the self-propulsion parameters D_θ and v_0 . Also, both the amplitude and persistence length of v_c decay with the increasing cluster size. Thus, the size of the active-passive cluster decreases

with increasing active particles in the system. Further, size of the active cluster can be estimated using Eq. (3). Again, with increasing η_a , *pushing effect* of active particles makes more free space for them. This leads to decrease of the active cluster size in the mixture.

Based on the above reasoning, a decreasing trend for the average cluster size with η_a is expected in the athermal condition. Simulation results presented in Fig. 6(a) show that $\langle N_c \rangle$ exponentially decays with η_a . The decay constant and the pre-exponential factor depend on the self-propulsion parameters as well as ρ_N . With increasing η_a , cluster number in the passive particle region does not change, however, in the active particle portion cluster numbers grow. Thus, the average cluster number almost linearly increases with adding active particles in the mixture. In the mixture most of the active particles exist as a single, as a result $\langle \eta_f \rangle$ remains unchanged with variation of the file composition unless η_a is large.

Cluster size distribution — $p(N_c)$, shown in Fig. 6(c), supports our assertion about formation of pure active, as well as, active-passive clusters. The size distribution function first exponentially decays, then slowly increases and decays again forming a plateau like structure, finally, a sharp peak appears in the large cluster size regime. These three segments of $p(N_c)$ provide a clear picture about the mixture structure.

Similar to an active single-file, the first segment of the distribution exponentially decreases with N_c . The associated decay constant is inversely proportional to $\sqrt{v_0 \tau_\theta}$ (not shown in the figures). Further, the decay constant grows with decreasing η_a . These features are attributed to the formation of clusters with active species only. The active particles push passive ones and make more free space available for them. Thus, the effective number density in the active segment of the file is much smaller than the passive part. If active swimmers are strong enough to aggregate passive species, effective density for the active part $\bar{\rho}_N \sim \eta_a \rho_N / [1 - (1 - \eta_a) \sigma \rho_N]$. Thus, the exponentially decaying part of $p(N_c)$ could be described by the Eq. (10). However, ρ_N there should be replaced by the effective density $\bar{\rho}_N$. Further, this estimation requires correction in v_0 unless it is large enough to sustain impact of passive species. This analytic argument well corroborates simulation results in Fig. 6(c).

After the initial decay, the increasing trend in $p(N_c)$ witnesses formation of clusters due to the pushing effect of active particles. As expected, the probability of forming such clusters with larger size increases with increasing passive fractions in the mixture. As the active particles can aggregate a finite number of particles, after a certain cluster size $p(N_c)$ decreases sharply.

The very sharp peak in $p(N_c)$ [at $N_c = N(1 - \eta_a)$, see Fig. 6(c)] is due to finite size of the simulation box. As a result of periodic boundary conditions, either end of the passive segment of the single-file encounters motile active species. Thus, all the passive particles can be aggregated forming a large cluster of size $N(1 - \eta_a)$.

The impact of the thermal fluctuations on the file

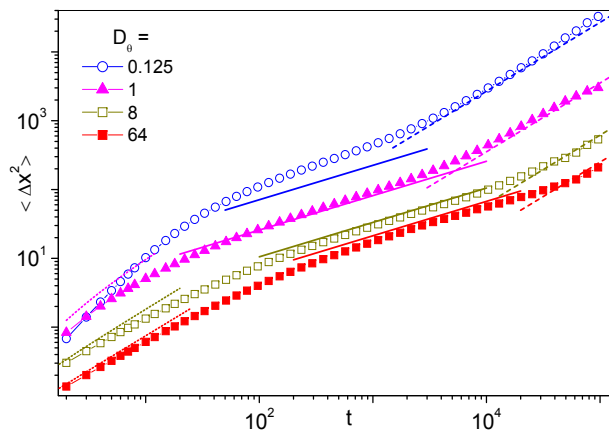


FIG. 8: (Color online) Mean square displacement $\langle \Delta x^2 \rangle$ as a function of time for different rotational diffusion constants (see legends). Three regimes of diffusion are fitted with analytic formulas. The dotted lines depict mean square displacement for the short regime based on the Eq. (12). Solid lines represent analytic estimation of sub-diffusion regime based on the Eq. (13). The long time normal diffusion regime is fitted with the formula $\langle \Delta x^2 \rangle = 2D_s t/N$. Other simulation parameters (unless reported otherwise in the legends): $v_0 = 1.0$, $\rho_N = 0.1$, and $D_0 = 0.03$.

structure is apparent from the Fig.7. Similar to the *Configuration I*, even very little thermal fluctuations break large clusters. With increasing η_a , effects of the thermal noise get suppressed when $v_0 \gg v_{th}$.

For the sake of simplicity we consider active and passive alike, they are of the same size. Thus, they encounter the same damping and have similar thermal diffusivity in the unconstrained situations. However, in general, active and passive species may not be of the same size. This would amount to the different thermal diffusivity and damping strength. A smaller passive particle encounters less damping, as a result, it can move more easily due to motility transfer from the motile swimmers. When a passive particle is smaller (larger) than active ones, more (less) number of passive particles can be aggregated by the pushing action of active species. This effect is equivalent to the increasing (decreasing) strength of self-propulsion.

IV. DIFFUSION

To understand diffusion of self-propelled particles as well as active-passive binary mixture as a single file, we calculate mean square displacement,

$$\langle \Delta x^2 \rangle = \sum_{i=1}^N \langle [x_i(t) - x_i(0)]^2 \rangle \quad (11)$$

$\langle \dots \rangle$ denotes averaging over a large number of independent stochastic realization. The mean square displacement $\langle \Delta x^2 \rangle$ as a function of t is plotted in Fig.8 for dif-

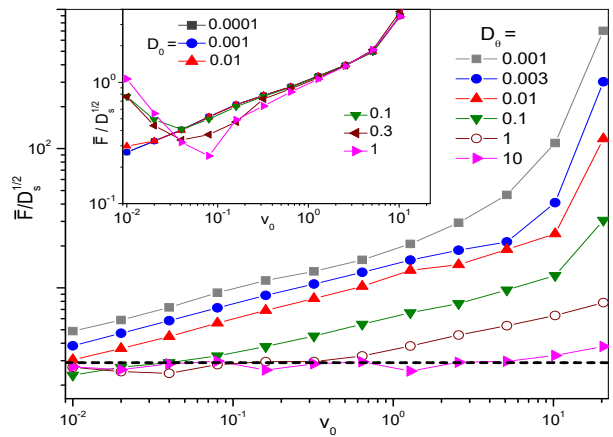


FIG. 9: (Color online) $\bar{F}/\sqrt{D_s}$ versus v_0 for different rotational diffusion (main panel) and the thermal translational diffusion (inset) as shown in the legends. Dashed line is the estimation based on Eq. (17). Simulation parameters unless mentioned in the legends: $\rho_N = 0.16$, $D_0 = 0$, and $D_\theta = 0.002$.

ferent rotational diffusion D_θ . Three distinct regions are apparently distinguished here. Initially, free diffusion of Janus particles (JPs) is observed with mean square displacement,

$$\langle \Delta x^2 \rangle = 2 \left(D_0 + \frac{v_0^2}{2D_\theta} \right) t + \frac{2v_0^2}{D_\theta^2} (e^{-D_\theta t} - 1) \quad (12)$$

As soon as particles meet neighboring ones, diffusion occurs under the constraint, particles cannot cross each other. Thus, a transition in $\langle \Delta x^2 \rangle$ versus t is observed after a certain time t_c which is the measure of the time to cross the average inter particle distance L/N . The transition time t_c depends on the particle density, particle size and diffusion of free Janus particles.

For $t > t_c$, the mean square displacement displays a sub-diffusive behavior,

$$\langle \Delta x^2 \rangle = \frac{2(1 - 2r_0\rho_N)F}{\rho_N} t^{1/2} \quad (13)$$

The mobility factor F is related to the single Janus particle diffusion constant D_s as, $F = \sqrt{D_s}/\pi$. The diffusion constant of a free Janus particle is given by,

$$D_s = D_0 + v_0^2/2D_\theta \quad (14)$$

The diffusion constant consists of two parts. The first term is the diffusion contribution due to thermal fluctuations. The pure thermal diffusion contribution can be computed by measuring the translational diffusion of a free JP in the absence of self-propulsion. The second part in Eq.(14) is the contribution of self-propulsion motion, directly proportional to the persistence time τ_θ and modulus of self-propulsion velocity v_0 .

In the Fig.8, the theoretical estimates of the mean square displacement in the normal diffusion and sub-diffusion regimes are depicted by dotted and solid lines,

respectively. For normal diffusion region, simulation results are in good agreement with analytic ones for all parameters. Also, in the sub-diffusion regime, analytic estimate based on the Eq.(13-14) is in accord with simulation for fast rotational diffusion of the JPs. However, the disagreement becomes noticeable for large self-propulsion persistence τ_θ . This attributes to the interference between stochastic and ballistic single file diffusion.

When the time is long enough for the tag particle to diffuse the length L normal diffusion region is recovered. This regime describes diffusion of the entire file as a whole. As if particles are strongly coupled and we are observing diffusion of the file's center of mass. Thus, mean square displacement is given by, $\langle \Delta x^2 \rangle = 2D_s t/N$.

A. Diffusion in a single file of active particles

For the all self-propulsion parameter regimes, in the long time limit and for very large L , the mean square displacement follows the relation,

$$\langle \Delta x^2 \rangle = 2\bar{F}t^{1/2}. \quad (15)$$

Where, \bar{F} is a function of the self-propulsion parameters in addition to the particle density ρ_N and intrinsic thermal transnational diffusion D_0 . In the Fig. 9 we plot the mobility \bar{F} (in the unit of $\sqrt{D_s}$) as a function of self-propulsion velocity for different rotational diffusion constant under athermal condition. The inset here represents impacts of D_0 in $\bar{F}/\sqrt{D_s}$ versus v_0 .

For a self-propulsion length larger than the average inter particle spacing, active particles preferably exist as clusters of different sizes. Simulation results in Fig. 9 show that for the diffusion of a tag particle buried in the cluster, the mobility is proportional to the $v_0^\alpha/D_\theta^{\beta_3}$ as long as $v_0 < v_0^c$. Where the exponents, $\alpha > 1$ and $\beta_3 > 0.5$. However, in the opposite limit, when the self-propulsion length is much smaller than the inter-particle spacing, particles in the 1D system preferably diffuse as a single particle with the constraint of single file. Particle dynamics here can be assumed as similar to the passive particle with effective temperature,

$$T_{eff} = \frac{\gamma}{k_B} \left(D_0 + \frac{v_0^2}{2D_\theta} \right). \quad (16)$$

Thus, under athermal condition the mobility factor becomes,

$$\bar{F} \rightarrow \frac{1 - \rho_N}{\sqrt{\pi\rho_N}}. \quad (17)$$

This estimation (indicated by dashed line in Fig. 9) is in well accord with simulation data when $l_\theta \ll 1/\rho_N$.

The inset in Fig. 9, depicts impact of thermal fluctuations on diffusion of active single file. Here, we consider the parameter regime with quite a slow rotational relaxation time so that movements are correlated for the entire

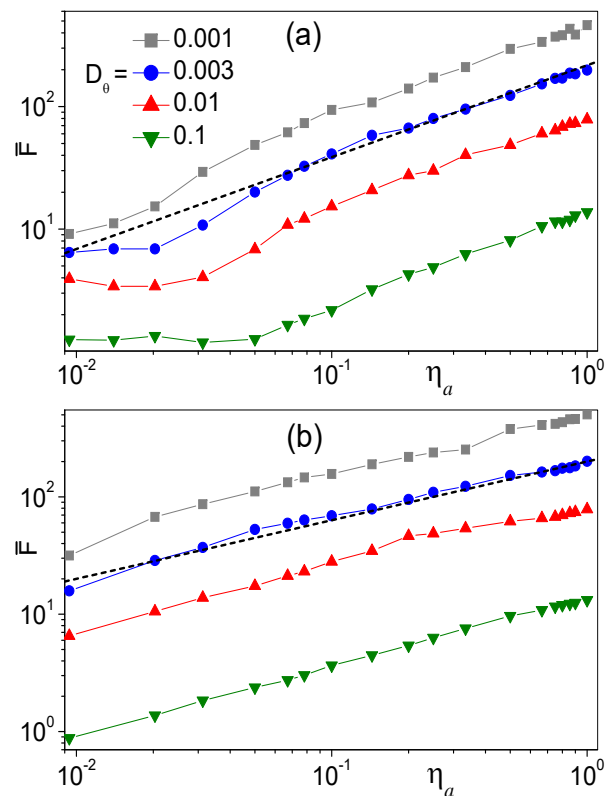


FIG. 10: (Color online) \bar{F} versus η_a for different rotational diffusion for two types of file configurations: (a) *Configuration I*: Active particles are uniformly distributed throughout the mixture; (b) *Configuration II*: Active particles are in the one side of the file and the other side contains passive particles only. The dashed line represents best fitted empirical relation, $\bar{F} = \bar{F}_0 \eta_a^\kappa$, with $\kappa = 0.75$ and 0.5 , respectively, for the configurations I and II. Simulation parameters unless mentioned in the legends: $\rho_N = 0.16$, $D_0 = 0$, and $v_0 = 1.0$.

range v_0 . Thermal fluctuation impact becomes noticeable when $D_0 > v_0^2/2D_\theta$. Note that for both in the thermal and athermal conditions, the mobility starts growing much faster with v_0 as soon as the self-propulsion velocity gets close to its critical value v_0^c . Recall that beyond the critical value, self-propulsion force is strong enough to make particles overlap each-other overcoming strong repulsion. It makes more space for free movement of the particles.

B. Diffusion in a single file of active-passive binary mixture

Simulation results in Fig. 10(a,b) depict diffusion of a tagged particle in the active-passive binary mixture. It should be noted that diffusion of a tagged particle, whatever it is active or passive one, displays similar traits. In the both types of configurations of active passive mixture, the diffusion of a tagged particle is greatly enhanced

with increasing fraction of active particle in the mixture. This attributes to the motility transfer of motile active particles to slowly diffusing passive particles[43].

For *configuration I*, where active particles are uniformly distributed throughout the mixture, initially with adding active particles the mobility \bar{F} is almost insensitive to η_a [see Fig. 10(a)]. Increasing the active fraction in the binary mixture beyond a certain value, mobility enhances monotonically. For quite large η_a , simulation data are best fitted with the empirical relation, $\bar{F} = \bar{F}_0 \eta_a^{0.75}$. It is depicted by a dashed line in Fig. 10(a).

On the other hand, when active particles are added from the one side to a single file of passive particles (*configuration II*), the mobility is a monotonically increasing function of η_a for the entire range of mixture composition. Best fitted empirical relation, $\bar{F} = \bar{F}_0 \eta_a^{0.5}$ [see Fig. 10(b)]. For the both configurations of the binary mixture, \bar{F}_0 is a function of self-propulsion parameters, D_θ and v_0 . Further, in the both configuration diffusion of the file considerably enhances through motility transfer mechanisms.

V. CONCLUSIONS

We have investigated the structural and diffusion properties of a mixture of active and passive colloidal particles of finite size in a single-file. The combination of self-propulsion and steric collisions results peculiar clustering in one dimension both in the pure active particle system, as well as, in the binary mixture. Our simulation results show that for the vanishingly small thermal fluctuations, when the self-propulsion length is larger than the average interparticle separation, active particles in a single file exist as clusters of various sizes. The average cluster size is a monotonic function of the self-propulsion length.

In the binary mixture a very similar clustering property is observed for *configuration I* when the fraction of active particles in the system is more than 10%. For very low active particle concentration, each active tracer forms clusters aggregating passive ones through pushing action. In this regime cluster size is insensitive to active species concentration. On the other hand, when active swimmers are added from one side of the mixture (*configuration II*), a much smaller number of clusters are formed and their size decay exponentially with increasing fraction of active particles in the mixture. For the both mixture configurations, cluster size is very sensitive to the thermal fluctuations even to a small extent.

Tagged particle diffusion in the single file of binary mixture exhibits sub-diffusive behaviour with $\langle \Delta x^2 \rangle = 2\bar{F}t^{1/2}$. Where, the mobility factor \bar{F} monotonically grows with increasing concentration of active particles in the mixture. This enhanced diffusion in the active-passive binary mixture witnesses motility transfer from the energetic active particles to the slowly moving passive ones.

We hope all our simulation results would be useful to synthesise active Janus particles with desired transport features and to operate them in a controlled manner for novel and emerging applications. In particular, to mention, targeted drug delivery, cleaning biological channels, and other emerging nano-technological and biomedical applications where particles diffuse through narrow channels with non-passing constraints.

Conflict of Interest

The authors declare no conflict of interest.

Data Availability Statement

The data that support the findings of this study are available on request from the corresponding author. The data are not publicly available due to privacy or ethical restrictions.

Acknowledgement

P.B. thanks UGC, New Delhi, India, for the award of a Junior Research Fellowship. P.K.G. is supported by SERB Core Research Grant No. CRG/2021/007394.

References

- [1] Harris T E 1965 Diffusion with "Collisions" between Particles *J. Appl. Prob.* **2** 323
- [2] Heckmann K 1972 *Biomembranes : Passive Permeability of Cell Membranes* (Plenum Press, New York) **3** p.127
- [3] Taloni A, Flomenbom O, Castañeda-Priego R and Marchesoni F 2017 Single file dynamics in soft materials *Soft Matter* **13** 1096
- [4] Lebowitz J L and Percus J K 1967 Kinetic Equations and Density Expansions: Exactly Solvable One-Dimensional System *Phys. Rev.* **155** 122
- [5] Levitt D G 1973 Dynamics of a Single-File Pore: Non-Fickian Behavior *Phys. Rev. A* **8** 3050
- [6] Nelissen K, Misko V R and Peeters F M 2007 Single-file diffusion of interacting particles in a one-dimensional channel *EPL* **80** 56004
- [7] Lucena D, Tkachenko D V, Nelissen K, Misko V R, Ferreira W P, Farias G A and Peeters F M 2012 Transition from single-file to two-dimensional diffusion of interacting particles in a quasi-one-dimensional channel *Phys. Rev. E* **85** 031147

- [8] Hodgkin A L and Keynes R D 1955 The potassium permeability of a giant nerve fibre *J. Physiol.* **128** 61
- [9] Richards P M 1977 Theory of one-dimensional hopping conductivity and diffusion *Phys. Rev. B* **16** 1393
- [10] Fedders P A 1978 Two-point correlation functions for a distinguishable particle hopping on a uniform one-dimensional chain *Phys. Rev. B* **17** 41
- [11] Alexander S and Pincus P 1978 Diffusion of labeled particles on one-dimensional chains *Phys. Rev. B* **18** 2011
- [12] Kärger J 1993 Long-time limit of the self-correlation-function of one-dimensional diffusion *Phys. Rev. E* **47** 1427
- [13] Berg H C 1984 *Random Walks in Biology* (Princeton University Press)
- [14] Haynes W M (ed.) 2011 *CRC Handbook of Chemistry and Physics* (CRC Press.)
- [15] Jobic H, Hahn K, Kärger J, Bée M, Tuel A, Noack M, Girnus I and Kearley G J 1997 Unidirectional and Single-File Diffusion of Molecules in One-Dimensional Channel Systems. A Quasi-Elastic Neutron Scattering Study *J. Phys. Chem. B* **101** 5834
- [16] Kukla V, Kornatowski J, Demuth D, Girnus I, Pfeifer H, Rees L V C, Schunk S, Unger K K and Kärger J 1996 NMR Studies of Single-File Diffusion in Unidimensional Channel Zeolites *Science* **272** 702
- [17] Lin B, Cui B, Lee J-H and Yu J 2002 Hydrodynamic coupling in diffusion of quasi-one-dimensional Brownian particles *EPL* **57** 724
- [18] Wei Q-H, Bechinger C and Leiderer P 2000 Single-file diffusion of colloids in one-dimensional channels *Science* **287** 625
- [19] Lutz C, Kollmann M and Bechinger C 2004 Single-file diffusion of colloids in one-dimensional channels *Phys. Rev. Lett.* **93** 026001
- [20] Chaki S, Chakrabarti R 2019 Enhanced diffusion, swelling, and slow reconfiguration of a single chain in non-Gaussian active bath *J. Chem. Phys.* **150** 094902
- [21] Goswami K, Chaki S and Chakrabarti R 2022 Reconfiguration, swelling and tagged monomer dynamics of a single polymer chain in Gaussian and non-Gaussian active baths *J. Phys. A: Math. Theor.* **55** 423002
- [22] Caprini L and Marconi U M B 2020 Time-dependent properties of interacting active matter: Dynamical behavior of one-dimensional systems of self-propelled particles *Phys. Rev. Research* **2** 033518
- [23] Dolai P, Das A, Kundu A, Dasgupta C, Dhar A and Kumar K V 2020 Universal scaling in active single-file dynamics *Soft Matter* **16** 7077
- [24] Paxton W F, Sundararajan S, Mallouk T E and Sen A 2006 Chemical locomotion *Angew. Chem. Int. Ed.* **45** 5420
- [25] Gibbs J G and Zhao Y-P 2009 Autonomously motile catalytic nanomotors by bubble propulsion *Appl. Phys. Lett.* **94** 163104
- [26] Howse J R, Jones R A L, Ryan A J, Gough T, Vafabakhsh R and Golestanian R 2007 Self-Motile Colloidal Particles: From Directed Propulsion to Random Walk *Phys. Rev. Lett.* **99** 048102
- [27] Volpe G, Buttinoni I, Vogt D, Kümmerer H-J and Bechinger C 2011 Microswimmers in patterned environments *Soft Matter* **7** 8810
- [28] Jiang H-R, Yoshinaga N and Sano M 2010 Active Motion of a Janus Particle by Self-Thermophoresis in a Defocused Laser Beam *Phys. Rev. Lett.* **105** 268302
- [29] Baraban L, Streubel R, Makarov D, Han L, Kar-naushenko D, Schmidt O G and Cuniberti G 2013 Fuel-Free Locomotion of Janus Motors: Magnetically Induced Thermophoresis *ACS Nano* **7** 1360
- [30] Ghosh P K, Vyacheslav M R, Marchesoni F and Nori F 2013 Self-Propelled Janus Particles in a Ratchet: Numerical Simulations *Phys. Rev. Lett.* **110** 268301
- [31] Ai B Q, Li Y-F and Zhong W-R 2014 Entropic Ratchet transport of interacting active Brownian particles *J. Chem. Phys.* **141** 194111
- [32] Gibbs J G and Zhao Y-P 2009 Autonomously motile catalytic nanomotors by bubble propulsion *Appl. Phys. Lett.* **94** 163104
- [33] Teeffelen S van and Löwen H 2008 Dynamics of a Brownian circle swimmer *Phys. Rev. E* **78**, 020101(R)
- [34] Kloeden P E and Platen E 1992 *Numerical Solution of Stochastic Differential Equations* (Springer: Berlin)
- [35] Matas-Navarro R, Golestanian R, Liverpool T B and Fielding S M 2014 Hydrodynamic suppression of phase separation in active suspensions *Phys. Rev. E* **90** 032304

- [36] Theers M, Westphal E, Qi K, Winkler R G and Gompper G 2018 Clustering of microswimmers: interplay of shape and hydrodynamics *Soft Matter* **14** 8590
- [37] Stürmer J, Seyrich M and Stark H 2019 Chemotaxis in a binary mixture of active and passive particles *J. Chem. Phys.* **150** 214901
- [38] J A-C and Golestanian R 2019 Active Phase Separation in Mixtures of Chemically Interacting Particles *Phys. Rev. Lett.* **123** 018101
- [39] Dolai P, Simha A and Mishra S 2018 Phase separation in binary mixtures of active and passive particles *Soft Matter* **14** 6137
- [40] Bag P, Nayak S, Debnath T and Ghosh P K 2022 Directed Autonomous Motion and Chiral Separation of Self-Propelled Janus Particles in Convection Roll Arrays *Phys. Chem. Lett.* **13** 11413
- [41] Ghosh P K, Zhou Y, Li Y, Marchesoni F and Nori F 2022 Binary Mixtures in Linear Convection Arrays *ChemPhysChem* **24** e202200471
- [42] Li Y, Zhou Y, Marchesoni F and Ghosh P K 2022 Colloidal clustering and diffusion in a convection cell array *Soft Matter* **18** 4778
- [43] Debnath D, Ghosh P K, Misko V R, Li Y, Marchesoni F and Nori F 2020 Enhanced motility in a binary mixture of active nano/microswimmers *Nanoscale* **12** 9717